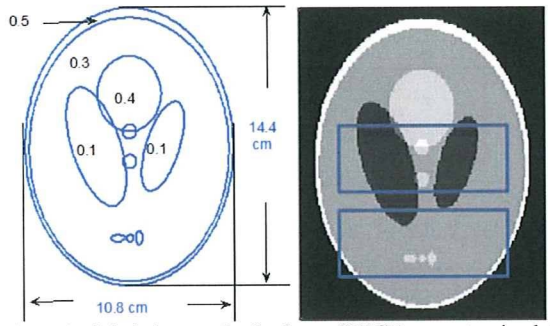

Figure 4 Digital phantom for fan-beam SPECT computer simulation. The square boxes in the right image indicate two regions-of-interest (ROIs).

In the reconstruction, first, differentiation followed by backprojection of truncated SPECT data was obtained. Then assuming the activity within a small part of the region-of-interest is known, the other part of the ROI was estimated using the PCOS method. The reconstructed image is shown in Fig. 5.

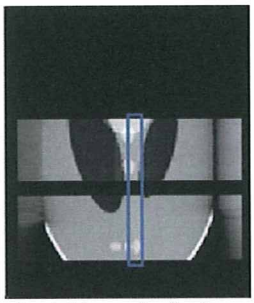

Figure 5: The reconstructed image for fan-beam geometry. The box indicates the region where the distribution is known *a priori.*

IV. Conclusion

This paper extended the work in [8] to SPECT imaging where uniform attenuation map is assumed. The interior problem was shown to be solvable given tiny *a priori* information. Reconstructions from simulated fan-beam data verify the theory.

The investigation of a pinhole system is presently undergoing. In the pinhole simulation, regularized maximum *a posteriori* (MAP) algorithm is used to reconstruct the simulated pinhole data. A low resolution reconstruction of the parallel beam collimated data is used as prior information.

References

[1] Iida H, Hayashida K, Nakazawa M and Katabuchi T, "Multicenter evaluation of quantitative SPECT reconstruction package – QSPECT & DTARG," *J. Nucl. Med.* 47 (Supplement 1), pp. 121, 2006.

[2] Rudzinski W, Swiat M, Tomaszewski M and Krejza J, "Cerebral hemodynamics and investigations of cerebral blood flow regulation," *Nucl Med Rev*, vol. 10, pp. 29-42, 2007.

[3] Imaizumi M, Kitagawa K, Hashikawa K, Oku N, Teratani T, Takasawa M, Yoshikawa T, Rishu P, Ohtsuki T, Hori M, Matsumoto M and Nishimura T, "Misery perfusion with split-dose ^{123}I-iodoamphetamine single-photon emission computed tomography in patients with carotid occlusive diseases," *Stroke*, vol. 33, pp. 2217-2223, 2002.

[4] Moriwaki H, Matsumoto M, Hashikawa K, Oku N, Ishida M, Seike Y, Fukuchi K, Hori M and Nishimura T, "Iodine-123-iomazenil and iodine-123-lodoamphetamine SPECT in major cerebral artery occlusive disease," *J Nucl Med*, vol. 39, pp. 1348-1353, 1998.

[5] Tsuchida T, Yonekura Y, Sadato N, Takahashi N, Yamamoto K and Ishii Y, "Prediction of improvement of cerebral perfusion with I-123 iomazenil SPECT," *Annals of Nucl. Med.,* vol. 13, pp. 265-268, 1999.

[6] Dargham A, Larulle M, Seibyl J, Rattner Z, Baldwin R M, Zoghbi S S, Zea-Ponce Y, Bremner J D, Hyde T M, Charney D S, Hoffer P B and Innis R B, "SPECT measurement of benzodiazepine receptors in human brain with iodine-123-iomazenil: kinetic and equilibrium paradigms," *J. Nucl. Med.,* vol. 35, pp. 228-238, 1994.

[7] Natterer F, *The Mathematics of Computerized Tomography* (SIAM), 1986.

[8] Kudo H, Courdurier M, Noo F and Defrise M, "Tiny *a proiri* knowledge solves the interior problem in computed tomography," *Phys. Med. Bio.*, vol. 53, pp. 2207-2231, 2008.

[9] Noo F, Clackdoyle R and Pack J D, "A two-step Hilbert transform method for 2D image reconstruction," *Phys. Med. Biol.,* vol. 49, pp. 3903-3923, 2004.

[10] Zou Y and Pan X, "Exact image reconstruction on PI-lines from minimum data in helical cone-beam CT," *Phys. Med. Biol.*, vol. 49, pp. 941-959, 2004.

[11] Pack J D, Noo F and Clackdoyle R, "Cone-beam reconstruction using the backprojection of locally-filtered projections," *IEEE Trans. Med. Imag.,* vol. 24, pp. 70-85, 2005.

[12] Pack J D and Noo F, "Cone-beam reconstruction using 1D filtering along the projection of M-lines," *Phys. Med. Biol.*, vol. 49, pp. 2317-2336, 2004.

[13] Ye Y and Wang G, "Filtered backprojection formula for exact image reconstruction from cone-beam data along a general scanning curve," *Med. Phys.*, vol. 32, pp. 42-48, 2005.

[14] Zou Y and Pan X, "Image reconstruction on PI-lines by use of filtered backprojection in helical cone-beam CT," *Phys. Med. Biol.,* vol. 49, pp. 2717-2731, 2004.

[15] Zou Y and Pan X, "An extended data function and its generalized backprojection for image reconstruction in helical cone-beam CT," *Phys. Med. Biol.*, vol. 49, pp. N3837, 2004.

[16] Huang Q, You J, Zeng G L and Gullberg G T, "Exact Reconstruction From Uniformly Attenuated Helical Cone-Beam projections in SPECT," LBNL Technical Report, LBNL-1359E, Lawrence Berkeley National Lab, Berkeley, USA., 2008.

[17] Huang Q, You J, Zeng G L, and Gullberg G T, "Reconstruction from uniformly attenuated SPECT partial-scan projection data using DBH method," IEEE Trans. Med. Imag., vol. 28, pp. 17-29, 2009.

[18] Noo F and Pack J D, "Theory for image reconstruction from divergent beam projections in SPECT," *IEEE Nuclear Science Symposium Conference Record*, vol. 6, pp. 3449-3452, 2006.

[19] Noo F, Defrise F, Pack J and Clackdoyle R, "Image reconstruction from truncated data in SPECT with uniform attenuation," *Inverse Problems*, vol. 23, pp. 645-667, 2007.

[20] Rullgard H, "An explicit inversion formula for the exponential Radon transform using data from 180 degrees," (Preprint in 2002 Sep) *Ark. Math.*, vol. 42, pp. 353-362, 2004.

[21] Liang Z, Ye J and Harrington D P, "Quantitative brain SPECT in three dimensions: an analytical approach without transmission scans," *Three-Dimensional Image Reconstruction in Radiology and Nuclear Medicine*, Kluwer Academic Publishers, pp. 117-132, 1996.

[22] Youla D C and Webb H, "Image restoration by the method of convex projections: Part I. Theory," *IEEE Trans Med. Imag.,* vol. 1, pp. 81–94, 1982.

A method to measure PET scatter fractions for daily quality control

H. W. de Jong[a)]
Department of Radiology and Nuclear Medicine, University Medical Centre, P. O. Box 85500, 3508 GA, Utrecht, The Netherlands and Department of Nuclear Medicine and PET Research, VU University Medical Centre, P. O. Box 7057, 1007 MB, Amsterdam, The Netherlands

M. Lubberink
Department of Nuclear Medicine and PET Research, VU University Medical Centre, P. O. Box 7057, 1007 MB, Amsterdam, The Netherlands

H. Watabe and H. Iida
Department of Investigative Radiology, National Cardiovascular Center Research Institute, 5-7-1 Fujishirodai, Suita, Osaka 565-8565, Japan

A. A. Lammertsma
Department of Nuclear Medicine and PET Research, VU University Medical Centre, P. O. Box 7057, 1007 MB, Amsterdam, The Netherlands

(Received 25 March 2009; revised 27 July 2009; accepted for publication 29 July 2009; published 14 September 2009)

Purpose: Regular monitoring of PET scanner performance is mandatory to assure quality of acquired data. While extensive performance measurements include many scanner characteristics such as resolution, count rate, uniformity, sensitivity, and scatter fraction (SF), most daily QC protocols are limited to uniformity and sensitivity measurements. These measurements may be too insensitive to detect more subtle drifts in detector gains that could lead to reduced detection of primary and increased detection of scattered events. Current methods to measure SF, such as those prescribed by the NEMA protocols (SF-NEMA), however, require specially designed phantoms and are too cumbersome to be performed on a daily basis.
Methods: In this study, a simple and versatile method to determine SF is described. This method (SF-DAILY) does not require additional measurements, making it suitable for daily QC. The method was validated for four different scanners by comparing results with those obtained with the NEMA 1994 protocol.
Results: For all scanner types and acquisition modes, excellent agreement was found between SF-NEMA and SF-DAILY.
Conclusions: The proposed method is a very practical and valuable addition to current daily QC protocols. In addition, the method can be used to accurately measure SF in phantoms with other dimensions than the NEMA phantom.
[DOI: 10.1118/1.3213096]

Key words: PET, scatter fraction, quality control, NEMA

I. INTRODUCTION

Assessment of PET scanner performance is mandatory to prevent image artifacts and to assure quantitative integrity of acquired data. In general, extensive performance measurements are performed only occasionally, e.g., after scanner installation, an upgrade, or major maintenance, with more concise quality control (QC) measurements being performed on a daily basis (daily QC). The purpose of this daily QC is to detect scanner malfunctioning and to monitor scanner stability. Ideally, this daily QC should be sensitive enough to detect changes in scanner performance that require (immediate) attention. As scanner maintenance may have substantial impact on patient throughput and planning, however, a decision to perform maintenance should be well founded, preferably based on a more extensive set of measured parameters. Therefore, it is important that daily QC tests provide as much relevant information as possible. Apart from offering a solid basis for decision making in clinical practice, daily QC data can also give insight in scanner behavior as a function of temperature, power loss, or time after maintenance.

While the above mentioned extensive (acceptance) performance measurements (using a range of different phantoms) include many scanner characteristics such as uniformity, sensitivity, and scatter fraction (SF), for practical reasons, the daily QC often is restricted to detector uniformity and sensitivity. These parameters are typically derived from a scan of a uniform cylindrical phantom filled with the long-lived isotope ^{68}Ge. These limited measurements may, however, obscure scanner drift or inaccuracies caused by changing detector gains, possibly leading to reduced detection of primary and increased detection of scattered events. In addition, drifts in electronics settings can lead to loss of sensitivity. For example, a shift in photomultiplier tube (PMT) gains can cause the 511 keV photopeak to drift, eventually (partly) falling outside the energy window.[1] This, in turn, may lead to a direct change in the detected SF, and hence image quality

and quantitative accuracy. Especially in state-of-the-art PET scanners that can only operate in 3D mode, SF is high (typically 50% of all detected events) and alterations in measured SF can have a major impact. In order to quantify 3D PET data, sophisticated scatter correction algorithms have been developed. If adjustments are not made while needed, however, changes in SF can cause the algorithm to over- or underestimate the scatter contribution, leading to bias, i.e., incorrect regional activity concentrations.

The SF is defined as the fraction of all events that have been scattered prior to detection. There are many ways to determine this SF, but the most widely accepted method is according to the NEMA standards. NEMA protocols have been established in a collaboration between scanner manufacturers and users. The advantage of NEMA protocols is that results can be interpreted by all parties, without uncertainties about the exact conditions under which measurements were performed. This is especially useful when communicating results between users, manufacturers, or other parties. Disadvantages of NEMA protocols are that they usually require specially designed setups and phantoms and that they are too cumbersome for use on a daily basis. Consequently, NEMA protocols often are used only for acceptance testing and in other situations where extensive measurements are required (e.g., following a major upgrade).

The purpose of the present study was to develop and validate a simple method to accurately estimate scatter fractions using a uniform cylindrical phantom. In general, a uniform cylindrical phantom is used to monitor sensitivity and uniformity on a daily basis and, therefore, this SF method could easily be added to the daily or weekly QC without the need for additional measurements. Validation was performed by comparing measured SF values with those derived according to the NEMA NU-1994 protocol using four different scanners.

II. MATERIALS AND METHODS

II.A. NEMA scatter fraction

NEMA standards for PET instrumentation describe a series of phantom measurements to determine scanner characteristics, including spatial resolution, scatter fraction, count rates, sensitivity, accuracy of correction methods, and general image quality. While the older NEMA-1994 protocol[1,2] was defined in a time when PET was primarily used as a brain imaging modality, the 2001 and 2007 protocols reflect the shift toward whole-body oncological applications.[3–6] For the SF measurement this is illustrated by the short 20 cm cylinder in the NEMA 1994 protocol (SF-NEMA1994) and the longer 70 cm cylinder in the NEMA 2001 protocol (SF-NEMA2001). The latter phantom was introduced to include scatter that originates from outside the axial field of view (FOV) of the scanner, and therefore SF-NEMA2001 is higher than SF-NEMA1994, especially when scanning in 3D mode (i.e., without septa in the FOV). In a comparative study, however, it was shown that a change in SF-NEMA1994 strongly correlated with a change in SF-NEMA2001.[3]

As the cylindrical daily QC phantom often has the same dimensions as the NEMA1994 scatter fraction phantom, SF-NEMA1994 was used as the gold standard for validating the proposed method. The NEMA1994 protocol describes a 20 cm diameter, 20 cm length, water filled cylinder in which a 20 cm line source can be inserted at three different positions (0, 45, and 90 mm from the center) (Fig. 1). After filling the line source with a low level of activity (~5 kBq/cc of ^{18}F), it was inserted at each of the three positions and, at each position, data were acquired for 15 min to ensure at least 200 kcounts per slice within the central 17 cm of the phantom.

SF-NEMA1994 was then obtained by (1) correcting the three measurements for ^{18}F decay, detector nonuniformities (normalization), and, where relevant, detector gaps (Fig. 1), (2) straightening the sinograms to eliminate curves due to off-center line source positions (Fig. 1), (3) setting all sinogram pixels corresponding to positions >12 cm from the center of the phantom to zero, (4) adding projection angles to create one profile per line source position, and (5) adding the three scatter profiles, thereby weighting for the annular region in which the line source is positioned, where (6) scattered events under the primary peaks were estimated using linear interpolation between count levels within 2 cm from the peak[2] (Fig. 1).

II.B. Simplified procedure

When acquiring PET data using a uniform cylindrical phantom of diameter D, filled with an arbitrary activity and placed centrally in the FOV, the resulting total count (T) projections are the sum of primary (or unscattered) events (P), scattered events (S), and random events. In general, randoms are corrected for by subtracting an independently measured estimate, usually obtained with the delayed window technique and therefore not addressed specifically in this study.[7] If r is the position on the projection (bin position) relative to the center of the FOV, then $S(r)$ is an arbitrary function describing the scatter background. The point spread function PSF(r) is a 1D function describing the resolution of the projection data centered around $r=0$ (Fig. 2). It is now postulated that, for a nonoblique projection plane, the spatial distribution of the total counts T of primary and scattered events within the FOV of a single ring of detectors (or nonoblique, direct plane) originating from a cylindrical phantom with diameter D is given by

$$T(r) = \mathrm{PSF}(r) \otimes (P(r,D,p) + S(r)),$$

$$P(r,D,p) = 2\sqrt{\frac{1}{4}D^2 - r^2}\cdot p \cdot \exp\left(-\mu\sqrt{\frac{1}{4}D^2 - r^2}\right), \quad r \le D,$$

$$P(r,D,p) = 0, \quad r > D, \tag{1}$$

where μ is the linear attenuation coefficient at 511 keV (cm^{-1}), $P(r,D,p)$ describes the distribution of the detected primary photons, and p is a scaling factor for the total number of detected primary photons that depends on both activity

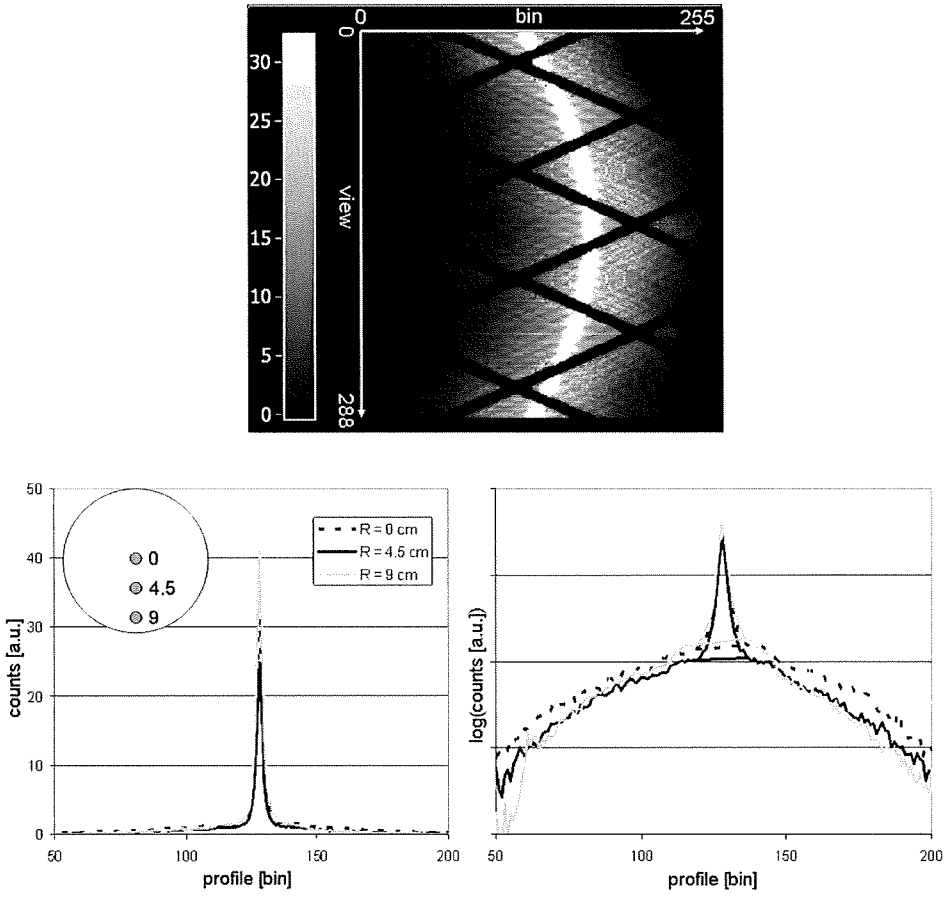

FIG. 1. Illustration of SF-NEMA procedure. The top image shows a sinogram from a line measurement for one of the three positions. Line profiles (bottom) are generated by straightening the profiles and averaging all views of the sinogram. Profiles are also shown using a logarithmic scale including the interpolated curves between ±2 cm (this case ±16 bins) from the center for scatter estimation. Using these curves primary and scatter fractions are extracted by integrating the profiles as described by the NEMA protocol.

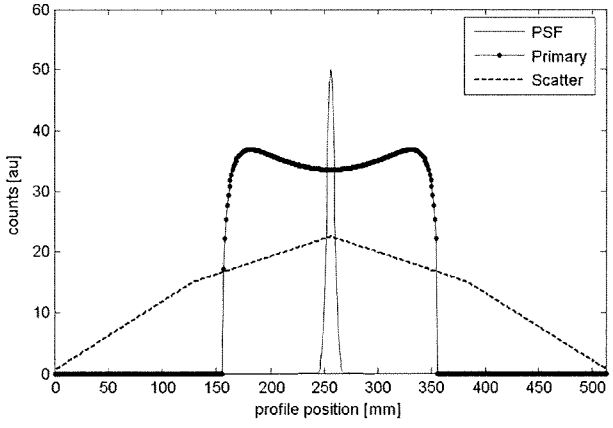

FIG. 2. Example of the three parts of the model used for estimating the SF-Daily: A PSF with a FWHM of 7 mm (scaled for illustration purposes), a primary response from a cylinder with a diameter of 20 cm, and an arbitrary scatter response.

in the phantom and sensitivity of the scanner. In short, the total response is a sum of primary and scatter events, where the shape of the primary contribution is known. In this case the activity of the nonoblique cross section through the cylindrical phantom was approximated by a circle [first term of $P(r,D,p)$], and multiplication with the attenuation factor (last exponential term) estimates the shape of the response in the absence of scattered photons.

In this study $S(r)$ was modeled as a first order cubic spline[8] based on a set of control points $(r_1,y_1;\ldots;r_n,y_n)$, i.e., $S(r)$ was simply modeled as a piecewise linear function between the coordinates (r_1,y_1) and (r_2,y_2), (r_2,y_2) and (r_3,y_3), and so on. Although a piecewise linear shape might not be natural, the convolution with PSF(r) removes discontinuities at the control points. Figure 2 gives an example of the components $P(r)$, $S(r)$, and PSF(r).

The new simplified method to derive SF (SF-Daily) makes direct use of Eq. (1). First, the PSF is modeled using a Gaussian function with a fixed width based on scanner specific resolution data. For the sake of simplicity, in all cases a spatially invariant resolution was assumed. Next, for the scatter function $S(r)$, the control points are chosen

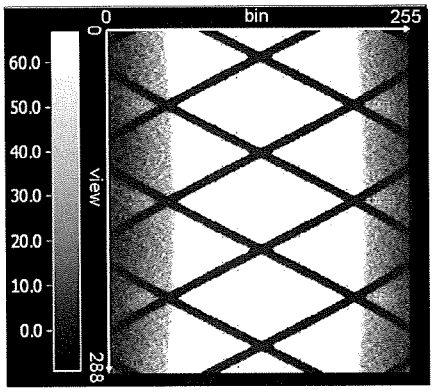

FIG. 3. Sinogram of uniform cylinder used for daily QC measurements. Scatter in the background of the sinogram is clearly visible. Black diagonal lines are due to gaps between detectors heads

equally divided over the data space (r direction) with r_1 located at the beginning and r_n at the end of the transversal field of view. For this study five control points were used. Since D, μ, and PSF(r) are known and $r_1,\ldots,r_5$ are fixed, $T(r)$ has p and the five base points $y_1,\ldots,y_5$ as free parameters. These parameters were estimated by fitting $T(r)$ to a measured response projection profile using a nonlinear curve fitting method (Levenberg-Marquardt[9]). It should be emphasized here that Eq. (1) is fitted to all projection data and not just to the tails of the sinogram, making the method very robust. For calculating SF only counts in the region $r \pm 3/5D$ are taken into account as this is prescribed by the NEMA protocol:

$$\mathrm{SF} = \frac{\int_{-3/5D}^{3/5D} S(r)dr}{\int_{-3/5D}^{3/5D} T(r)dr}. \tag{2}$$

To acquire data, a uniformly filled cylindrical phantom with known diameter (in the present case 20 cm for the whole-body scanners and 4.5 cm for the animal scanner) has to be placed in the center of the FOV, with its long axis in line with the scanner axis. In case the scanner has scintillation crystals containing intrinsic radioactivity such as L(Y)SO, background radiation has to be taken into account, as it produces randoms and a small fraction of true coincidences due to cascading gamma rays.[10] This background activity, however, usually is very low (typically less than 1×10^{-5} counts per second per line of response). On the other hand care should be taken not to induce pileup effects that can alter SF due to high count rates. Although this differs from scanner to scanner, as an example, SF for the high resolution research tomography (HRRT) is stable when total activity in the FOV is between approximately 1 and 100 MBq.[11] Although the count rate has negligible effect on SF as long as it is kept within the clinical range, ideally, total activity in the cylinder should be comparable to that used for the NEMA protocol (2.5 kBq cc^{-1}, or 15 MBq). Figure 3 shows an example of an acquired sinogram.

II.C. Scanners

To test and validate the new SF-Daily method under various circumstances, data from four different PET scanners were used. The scanners varied in crystal material, crystal size, ring diameter, and axial field of view, characteristics that all affect the scatter fraction. Table I gives an overview of relevant scanner data.

The Siemens HR (also known as ECAT Exact 47)[12] is a whole-body BGO scanner that can be operated in both 2D and 3D modes by means of retractable septa. Although 3D acquisitions yield higher sensitivity, the 2D mode is characterized by smaller randoms and scatter fractions, which can be advantageous for high count rate studies. The Philips Allegro[13] is a 3D only whole-body scanner based on curved GSO crystals, which have the advantage of a relatively high energy resolution compared with other PET crystals, resulting in a lower SF. The 3D only Siemens HRRT was one of the first scanners to apply LSO crystals. Its high spatial resolution enables detailed brain studies and small animal applications that can be covered in one bed position, thanks to the large axial FOV.[11] The Siemens microPET Focus 120 (Ref. 14) is a dedicated small animal LSO scanner with a gantry opening of approximately 20 cm. Although a new NEMA protocol specifically for small animal PET scanners was introduced only recently[15] microPET experiments using NEMA-like phantoms have already been reported previously.[16] Table I also lists resolution data (mm FWHM) as used for modeling PSF in Eq. (1).

II.D. Scatter fraction measurements

SF-NEMA and SF-Daily were measured and compared for all four scanners. For the HR, SF was measured using a cylinder, filled with ^{18}F, in both 2D and 3D acquisition modes. This provided a means to evaluate the effects of septa on measured SF for both methods. Although in most cases 3D sinograms were acquired, analysis was performed only on nonoblique (direct) planes in the sinogram. Hence, all

TABLE I. Relevant data of the various scanners.

Scanner	Crystal material	Crystal thickness (mm)	Axial FOV (cm)	Diameter gantry (cm)	Resolution used (mm FWHM)	Ring diameter (cm)
Siemens HR	BGO	30	15	51	5	82.7
Philips Allegro	GSO	20	18	56	5	86.4
Siemens HRRT	LSO	20	25	31	3	46.9
Siemens microPET Focus 120	LSO	10	7.6	20	2	25.8

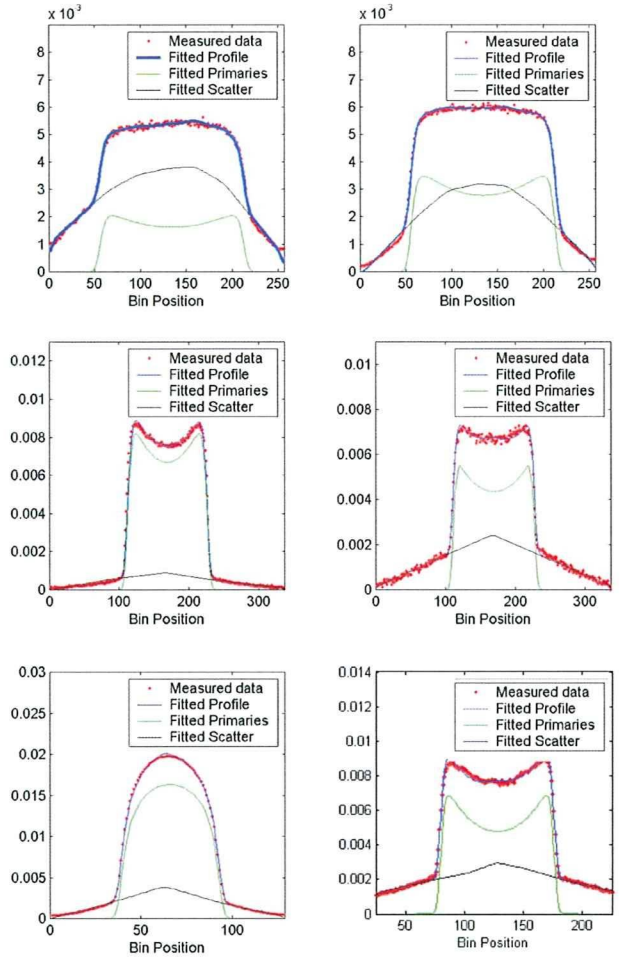

FIG. 4. Profiles of measured and fitted data. Top: HRRT before (left) and after (right) scanner setup. Mid: HR in 2D (left) and 3D (right) acquisition mode. Bottom: MicroPET (left) and Allegro (right). Due to the normalization process vertical units are arbitrary.

oblique planes (also called segment 1 and higher) were disregarded, effectively resulting in a 2D sinogram.

For the HRRT, SF-Daily was measured using a ^{68}Ge phantom (diameter of 20 cm, length of 27 cm, 20 MBq), routinely used for daily QC purposes. Sensitivity of SF-NEMA to small changes in SF was investigated by measuring SF of the HRRT just before and after performing a setup process (i.e., tuning of gain and other settings in order to maximize performance), as this setup process will decrease SF due to optimized energy calibration. SF was measured for the whole gantry and plane by plane. To assess effects of noise, SF-Daily for the whole gantry was measured using acquisition times of 15, 2, and 1 min.

For the Allegro, SF was determined for different lower energy threshold settings (260, 310, 360, and 410 keV) and an upper level discriminator set to 665 keV in order to investigate the correlation between both SF methods. For this a 20 cm diameter, 20 cm length cylinder filled with 20 MBq ^{18}F was used. As no mini-scatter-phantom was available for the microPET Focus 120, only SF-Daily was measured using a cylinder with an inner radius of 4.5 cm and a length of 10 cm, filled with 10 MBq, and this measurement was compared with published SF-NEMA values.[4]

TABLE II. Comparison of SF-NEMA and SF-Daily.

Scanner	SF-NEMA (%)	SF-Daily (%)
HRRT before setup	63	63
HRRT after setup	50	51
HRRT 15 min	50	51
HRRT 2 min	50	50
HRRT 1 min	50	50
HR 2D	14	13
HR 3D	38	33
MicroPET 45mm diameter cylinder	27[a]	23
Allegro	36	34

[a]The SF-NEMA was determined for a 60 mm phantom (8).

III. RESULTS

Sinogram profiles of the central axial plane and SF-Daily curve fits of total response $T(r)$ according to Eq. (1) are shown in Fig. 4 for all scanners. In addition, resulting primary $P(r)$ and scattered events $S(r)$ are shown. In all cases, the analytical response function equation (1) could be fitted to the data with high accuracy. Clearly, both shape and amplitude of the scatter distribution differ among scanners and acquisition modes. The HRRT setup process resulted in a lower SF and a more symmetric scatter distribution. Differences in scatter contribution between 2D and 3D modes are clearly illustrated by the HR profiles. The HR in 3D mode and the Allegro (measured using the lower level discriminator set at 410 keV) have similar profiles, indicating the impact of scanner geometry. The shape of the fitted primaries of the microPET deviates substantially from that of the other scanners due to the much smaller size of the phantom used. In general, SF measurement using SF-Daily were relatively insensitive to changes in PSF. Typically, doubling PSF (e.g., from 5 to 10 mm) resulted in only a 10% change in SF-Daily.

Table II summarizes SF values as obtained with SF-Daily and SF-NEMA. In addition, in case of the HRRT, SF values for different noise levels are included. Plane-by-plane SF values for the HRRT are shown in Fig. 5.

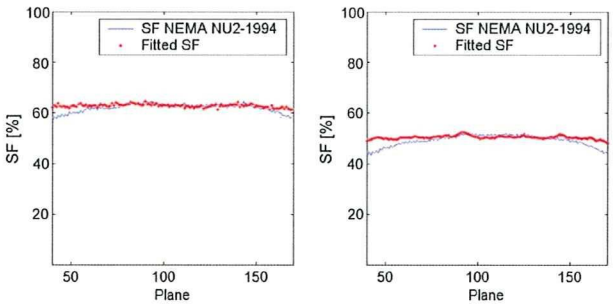

FIG. 5. Plane-by-plane values of SF-NEMA and SF-Daily (fitted SF) for the HRRT before (left) and after (right) setup.

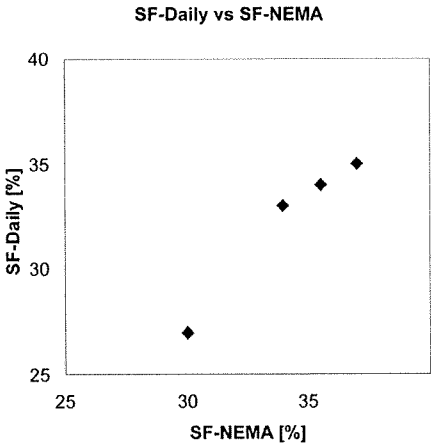

FIG. 6. SF-Daily and SF-NEMA values measured on the Allegro. Data points with higher SF refer to measurements with lower threshold values (260, 310, 360, and 410 keV).

Figure 6 shows SF values of the Philips Allegro for varying lower energy threshold settings. Both SF-NEMA and SF-Daily increased slightly with decreasing threshold channel, and a good correlation between both methods was found (R^2=0.96). Finally, Fig. 7 shows a Bland-Altman plot of the combined results presented in Table II and Fig. 6.

IV. DISCUSSION AND CONCLUSION

Using a simple curve fitting method, SF-Daily values were determined for different scanners and acquisition modes and compared to SF-NEMA values. A difference between SF-Daily and SF-NEMA only existed for the HR in 3D mode and for the microPET. For the latter, however, SF-Daily was measured using a cylinder with an inner diameter of 4.5 cm, while published SF-NEMA data were obtained with a cylinder of 6 cm diameter. The impact of noise was negligible for the three acquisition times investigated. The count rate in the HRRT scans was approximately 50 kcounts per slice, resulting in more than 100 counts per bin in the 1 min profiles, apparently sufficient for an accurate fit. The

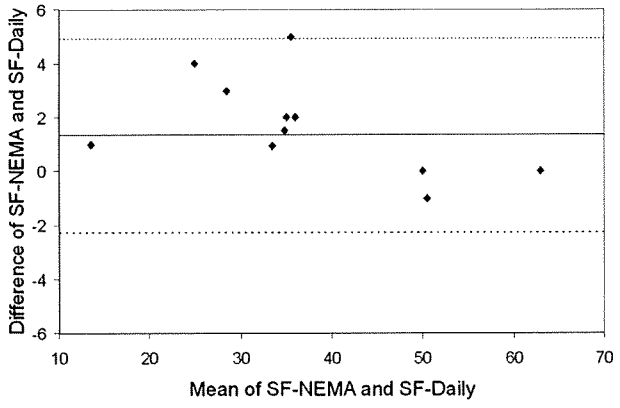

FIG. 7. Blant-Altman plot of all SF data from all four scanners and scan modes (data from Table II).

plane-by-plane comparison of SF-Daily and SF-NEMA showed good agreement especially in the center of the FOV. The slight deviation for the outer planes is probably due to the slightly longer phantom used for SF-Daily than for SF-Daily.

In general, slight deviations in fitted and acquired profiles could be seen, especially at the maxima of the response (Fig. 4). Most likely these deviations are due to the fact that the thickness of the wall of the cylinder was not taken into account. Nevertheless, they have negligible effect on the resulting SF.

Similar to SF-NEMA, SF-Daily can be performed on either only a subset of the total sinogram, e.g., only on nonoblique (direct) planes, or on all sinogram planes/segments via a rebinning step.[5] The latter requires slight adaption of Eq. (1), as the primary response in oblique planes will be based on an oblique cross section of the phantom (in case of a cylinder this will become an ellipse) rather than a circle. In this study SF values were only determined using direct (2D) sinograms for both the SF-NEMA and SF-Daily methods. For one scanner these sinograms were derived from data acquired in both 2D mode (with septa) and 3D mode (without septa) in order to test different levels of scatter and randoms.

Although the SF-Daily method does require that the phantom is positioned in the center of the FOV, in practice it proved to be insensitive to slight misplacements. The method could, however, easily be extended with an algorithm to align the sinogram, similar to the SF-NEMA requirement.

One limitation is that not all scanners use cylindrical phantoms for daily QC purposes but rely on measurements of small sources in air. Although this has the benefit of requiring less activity, it gives the energy resolution at 511 keV rather than the scatter fraction. Furthermore, use of a point source in air also prohibits measurement of uniformity of coincidence timing over a large area of the FOV.

It should be emphasized that SF-Daily fits a profile to all projection data. This is in contrast to some scatter correction methods[17] that rely on fitting the tails of the scatter profile. In the presented approach all data are used and that knowledge about the primary response is included, making the method robust and insensitive to noise.

In general, SF-Daily values obtained were in close agreement with those derived using the NEMA protocol, making the method sufficiently sensitive to detect small changes in SF. Because the shape of the primary distribution is well known, accurate fits of the sum of scatter and primary events to the total profile can be achieved, without making prior assumptions about the shape of the scatter distribution. Furthermore no discontinuities in the estimated responses $S(r)$ were found. The method is also suitable for determining SF values in case of "dirty" radionuclides (i.e., radionuclides that emit gamma rays in addition to positrons),[18] activity outside the FOV, and phantoms with deviating dimensions, as long as the exact dimensions are known.

In conclusion, as this method does not require measurements with special phantoms, it can be used to accurately

monitor SF using both arbitrarily sized cylindrical phantoms and short acquisition times, making the method particularly useful for daily QC purposes.

[a]Author to whom correspondence should be addressed. Electronic mail: h.w.a.m.dejong@umcutrecht.nl; Telephone: +31-(0)88-7553327.

[1]G. Brix *et al.*, "Performance evaluation of a whole-body PET scanner using the NEMA protocol," J. Nucl. Med. **38**, 1614–1623 (1997).
[2]National Manufacturers Association, NEMA Standards Publication No. NU 2-1994 (National Manufacturers, Washington, DC, 1994).
[3]M. E. Daube-Witherspoon *et al.*, "PET performance measurements using the NEMA NU 2-2001 standard," J. Nucl. Med. **43**, 1398–1409 (2002).
[4]H. Herzog, L. Tellmann, C. Hocke, U. Pietrzyk, M. E. Casey, and T. Kuwert, "NEMA NU2-2001 guided performance evaluation of four Siemens ECAT PET scanners," IEEE Trans. Nucl. Sci. **51**, 2662–2669 (2004).
[5]National Manufacturers Association, NEMA Standards Publication No. NU 2-2001 (National Electrical Manufacturers, Washington, DC, 2001).
[6]National Manufacturers Association, NEMA Standards Publication No. NU 2-2007 (National Electrical Manufacturers, Washington, DC, 2007).
[7]E. J. Hoffman, S. C. Huang, M. E. Phelps, and D. E. Kuhl, "Quantitation in positron emission computed tomography: 4. Effect of accidental coincidences," J. Comput. Assist. Tomogr. **5**, 391–400 (1981).
[8]C. de Boor, *A Practical Guide to Splines* (Springer-Verlag, New York, 1978).
[9]D. Marquardt, "An algorithm for least-squares estimation of nonlinear parameters," SIAM J. Appl. Math. **11**, 431–441 (1963).
[10]C. C. Watson, M. E. Casey, L. Eriksson, T. Mulnix, D. Adams, and B. Bendriem, "NEMA NU 2 performance tests for scanners with intrinsic radioactivity," J. Nucl. Med. **45**, 822–826 (2004).
[11]H. W. de Jong, F. H. van Velden, R. W. Kloet, F. L. Buijs, R. Boellaard, and A. A. Lammertsma, "Performance evaluation of the ECAT HRRT: An LSO-LYSO double layer high resolution, high sensitivity scanner," Phys. Med. Biol. **52**, 1505–1526 (2007).
[12]K. Wienhard *et al.*, "The Ecat exact HR—Performance of a new high-resolution positron scanner," J. Comput. Assist. Tomogr. **18**, 110–118 (1994).
[13]S. Surti and J. S. Karp, "Imaging characteristics of a 3-dimensional GSO whole-body PET camera," J. Nucl. Med. **45**, 1040–1049 (2004).
[14]J. S. Kim *et al.*, "Performance measurement of the microPET Focus 120 scanner," J. Nucl. Med. **48**, 1527–1535 (2007).
[15]National Manufacturers Association, "Performance measurements of small animal positron emission tomographs," NEMA Standards Publication No. NU 2-2008 (National Electrical Manufacturers, Washington, DC, 2008).
[16]Y. C. Tai *et al.*, "Performance evaluation of the microPET Focus: A third-generation microPET scanner dedicated to animal imaging," J. Nucl. Med. **46**, 455–463 (2005).
[17]C. C. Watson, "New, faster, image-based scatter correction for 3D PET," IEEE Trans. Nucl. Sci. **47**, 1587–1594 (2000).
[18]M. Lubberink, S. A. van, H. W. de Jong, G. A. van Dongen, and G. J. Teule, "Acquisition settings for PET of 124I administered simultaneously with therapeutic amounts of 131I," J. Nucl. Med. **47**, 1375–1381 (2006).

動物実験手技集成

監修　寺本　昇

国立循環器病センター　研究所　先進医工学センター　放射線医学部

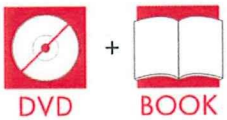

NTS

動物実験手技集成

CONTENTS

監修・解説：
国立循環器病センター　研究所
先進医工学センター　放射線医学部
寺本 昇

（取り扱いのご注意）
●ディスクは両面とも、指紋、汚れ、キズなどをつけないように取り扱ってください。
●ディスクが汚れたときは、メガネふきのようなやわらかい布を軽く水で湿らせ、内側から外側に向かって放射状に軽くふきとってください。レコード用クリーナーや溶剤等は使用しないでください。
●ディスクは両面共、鉛筆、ボールペン、油性ペン等で文字や絵を描いたり、シール等を貼付しないでください。
●ひび割れや変形、または接着剤等で修復されたディスクは危険ですから絶対に使用しないでください。また静電気防止スプレー等の使用は、ひび割れの原因となることがあります。
（保管上のご注意）
●使用後は、必ずプレーヤーから取り出し、DVD専用ケースに納めて、直射日光の当たるところや高温多湿の場所は避けて保管してください。
●ディスクケースの上に重いものを置いたり、落としたりすると、ケースが破損し、ケガをすることがあります。

株式会社 エヌ・ティー・エス
〒113-0034　東京都文京区湯島2-16-16
TEL.03-3814-9151　FAX.03-3814-9152
http://www.nts-book.co.jp/

NTSNM-00004	レンタル禁止	NTSC 日本市場向
片面・一層	モノラル	
COLOR MPEG-2	DOLBY DIGITAL	4:3
複製不能